ROYAL SOCIETY
OF CHEMISTRY

Check for updates

Hierarchical NiCo$_2$O$_4$ nanosheets on carbon nanofiber films for high energy density and long-life Li–O$_2$ batteries†

Guoxue Liu, Lei Zhang,* Suqing Wang, Liang-Xin Ding and Haihui Wang ![ORCID]*

Designing oxygen cathodes with both high energy density and excellent cycling stability is a great challenge in the development of lithium–oxygen (Li–O$_2$) batteries for energy storage systems. Herein, we design a novel structure of hierarchical NiCo$_2$O$_4$ nanosheets on porous carbon nanofiber films (denoted as NiCo$_2$O$_4$@CNFs) as an oxygen cathode for lithium–oxygen batteries. The NiCo$_2$O$_4$@CNFs cathode delivers a high specific discharge capacity of 4179 mA h g^{-1}, a high energy density of 2110 W h kg^{-1} and superior cycling stability over 350 cycles. The excellent electrochemical performance of the NiCo$_2$O$_4$@CNFs cathode can be attributed to the rational design and engineering of catalysts and porous conductive electrodes. These results indicate that the NiCo$_2$O$_4$@CNFs electrode is a promising candidate for high energy density and long-life Li–O$_2$ batteries. Additionally, the rational design of the hierarchical catalyst constructed low-dimensional nanostructure and the lightweight porous carbon nanofiber electrode can be also used for other metal–oxygen batteries, such as zinc–oxygen (Zn–O$_2$) batteries, aluminum–oxygen (Al–O$_2$) batteries, and sodium–oxygen (Na–O$_2$) batteries.

Rechargeable lithium–oxygen (Li–O$_2$) batteries are unmatched candidates amongst future electrochemical energy storage devices for electric vehicles due to their high theoretical energy density of 3505 W h kg^{-1}, which is about 10 times higher than that of conventional Li-ion batteries (360 W h kg^{-1}).[1–6] In a typical prototype, a Li–O$_2$ battery is composed of an Li$^+$ conducting electrolyte, a separator, a lithium anode, and a porous O$_2$ breathing cathode, and its cycling mechanism is based on the oxygen reduction reaction (ORR) and the oxygen evolution reaction (OER) between Li$^+$ and oxygen on the cathode: $2Li^+ + O_2 + 2e^- \leftrightarrow Li_2O_2$.[7,8] As a result, the key of the development of high-performance Li–O$_2$ batteries depends on the cathode, which needs to meet such requirements: highly active bifunctional ORR/OER catalysts, and porous conductive electrodes for

oxygen diffusion and electron transport, as well as offering enough space to meet the needs of Li$_2$O$_2$ deposition.[9–12]

Despite their superior theoretical storage capacity, constructing cycling stable Li–O$_2$ battery cathodes is still facing materials challenges.[11,13] This is traced to the sluggish kinetics of the ORR/OER giving large discharge/charge overpotentials and the random deposition of Li$_2$O$_2$ blocking the permeation path for oxygen and the electrolyte, leading to low round-trip efficiency, poor rate capability, and short cycling performance.[9,14] From the catalyst point of view, although the most efficient catalysts for the sluggish bifunctional ORR/OER are still noble metals,[15–19] low cost earth-abundant transition metal oxides, such as MnO$_2$,[20–23] NiCo$_2$O$_4$,[24,25] Co$_3$O$_4$,[26–28] MnCo$_2$O$_4$,[29,30] and CoMn$_2$O$_4$,[31,32] are preferred for practical application. Among these, NiCo$_2$O$_4$-based materials have received considerable attention due to their rich redox reaction sites from both redox couples of Co^{3+}/Co^{2+} and Ni^{3+}/Ni^{2+}, good electrical conductivity, and affordable cost.[33–35] Hence, low-dimensional nanostructured NiCo$_2$O$_4$-based catalysts, such as 0D nanoparticles, 1D nanorods/nanowires/nanotubes and 2D nanosheets, have been reported as bifunctional ORR/OER catalysts for rechargeable Li–O$_2$ batteries.[36–41] Low dimensional NiCo$_2$O$_4$ nanostructures possess highly exposed active sites and short diffusion length for the ORR/OER, which can lead to a high discharge capacity and low overpotentials.[36] However, these low-dimensional nanostructures cannot ensure enough space for solid Li$_2$O$_2$ deposition, which could cover catalytically active sites and result in poor cycling performance.[24] Also, the mass transport channels of Li$^+$ and oxygen are easily clogged due to relatively small pores of low-dimensional nanostructures, leading to cell failure.[42] Therefore, the fabrication of NiCo$_2$O$_4$-based catalysts with efficiently sufficient space and an accessible porous structure is highly desirable for Li–O$_2$ batteries.

As to the porous conductive electrode, a "binder-free" cathode has recently been introduced as an ideal electrode to avoid the side reaction between the binder and electrolyte.[43] Among the substrates, Ni foam and carbon textile are most commonly used because of their good breathability, high

School of Chemistry and Chemical Engineering, South China University of Technology, Guangzhou 510640, China. E-mail: celeizhang@scut.edu.cn; hhwang@scut.edu.cn

conductivity and good stability. For example, Liu *et al.* synthesized a cathode of δ-MnO_2 assembled by ultrathin nanosheets on Ni foam coated with graphene, which showed excellent stability to enhance the cycling stability of Li–O_2 batteries.[23] Zhang *et al.* described that TiO_2 nanowires grown on carbon clothes exhibited good electrochemical performance attributed to their high mechanical and chemical stability.[44] However, the high mass densities of Ni foam and carbon textile will lead to sacrificing capacity and energy density.[39] Thus, it is highly demanded to design and develop a lightweight cathode with high catalytic ORR/OER activities for realizing the high energy density of Li–O_2 batteries.

To achieve a Li–O_2 battery with high cycling stability and high energy density, it is highly necessary to combine a rationally structured catalyst and a lightweight porous conductive electrode. Herein, we propose a novel structure of hierarchical $NiCo_2O_4$ nanosheets on porous carbon nanofiber films (denoted as $NiCo_2O_4$@CNFs), for high energy density and long-life Li–O_2 batteries. The nanostructured cathode integrates several desirable design rationales for high-performance Li–O_2 batteries based on low-dimensional ultrathin nanosheets, lightweight conductive carbon networks, and a binder-free cathode. With the help of this rational design, the $NiCo_2O_4$@CNFs cathode exhibits excellent electrochemical performance including a high specific discharge capacity of 4179 mA h g^{-1}, an excellent energy density of 2110 W h kg^{-1}, and especially superior cycling stability over 350 cycles.

The fabrication procedure of porous $NiCo_2O_4$ nanosheets on carbon nanofiber films and the structure of the Li–O_2 battery are described in Fig. 1. Typically, porous carbon nanofiber films were prepared *via* a facile electrospinning technique followed by carbonization. In step I, Ni–Co precursor nanosheets were grown on carbon nanofiber films by a hydrothermal method to form core–shell structures. In step II, the Ni–Co precursor nanosheets were transformed into porous $NiCo_2O_4$ nanosheets through annealing and the $NiCo_2O_4$@CNFs cathode was finally

obtained. The morphology and microstructure of the cathode were investigated by field emission scanning electron microscopy (FESEM). As shown in Fig. 2, the randomly arranged carbon nanofibers form conductive networks with numerous irregular micrometer-scale pores between the carbon nanofibers, which could enhance electron transfer among cathodes and offer sufficient channels for cathode breathing. From the high magnification SEM, it can be seen that the as-prepared carbon nanofibers have an average diameter of about 180 nm with a smooth surface (Fig. 2b). The X-ray diffraction (XRD) pattern of CNFs shows no obvious diffraction peaks, indicating that the carbon nanofibers consist of typical amorphous carbon (Fig. S1, ESI†). Afterwards, Ni–Co precursors were grown on carbon nanofibers through a simple hydrothermal method. As shown in Fig. 2c and d, the low-magnification FESEM image of $NiCo_2O_4$@CNFs (Fig. 2c) displays that the Ni–Co precursor nanosheets uniformly coat the carbon nanofibers and the pores between the individual carbon nanofibers are not been covered. The magnified FESEM image (Fig. 2d) shows that the Ni–Co precursor nanosheets are around 10 nm thick. After annealing at 350 °C in a nitrogen atmosphere, the Ni–Co precursor nanosheets were converted to $NiCo_2O_4$ nanosheets. From the FESEM images (Fig. 2e), it can be clearly observed that the $NiCo_2O_4$ shell is still constructed by nanosheet-like subunits on the carbon nanofibers because of the robust support of the carbon nanofibers. Interestingly, from the FESEM image of a single 1D $NiCo_2O_4$@CNFs (Fig. 2f), the $NiCo_2O_4$ nanosheets are clearly observed with a rough and porous surface.

The crystallographic phase of the $NiCo_2O_4$ nanosheets was characterized by X-ray powder diffraction (XRD), as shown in Fig. S2 (ESI†). All of the diffraction peaks in the XRD pattern can be unambiguously assigned to the spinel $NiCo_2O_4$ (JCPDS no. 20-0781).[24,34] No other diffraction peaks from possible impurities are observed, suggesting that the Ni–Co precursor is converted into highly pure spinel $NiCo_2O_4$. By thermogravimetric analysis (TGA, Fig. S3, ESI†), the mass content of $NiCo_2O_4$ in $NiCo_2O_4$@CNFs is approximately 40%.[36,39] The chemical
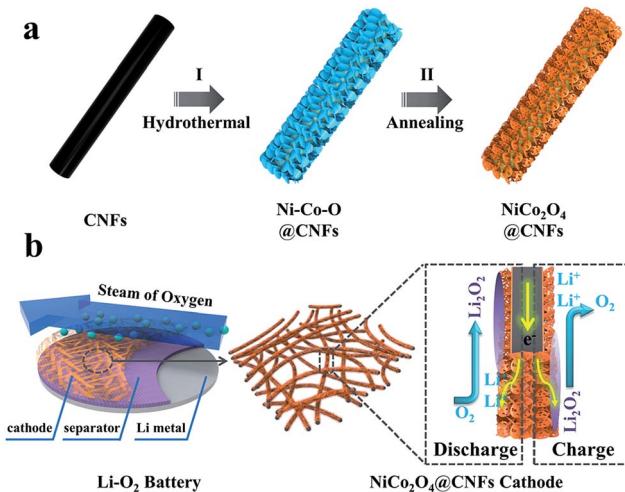
Fig. 1 (a) Schematic illustration of the fabrication of the $NiCo_2O_4$@CNFs cathode; (b) structure of the rechargeable Li–O_2 battery containing this cathode.
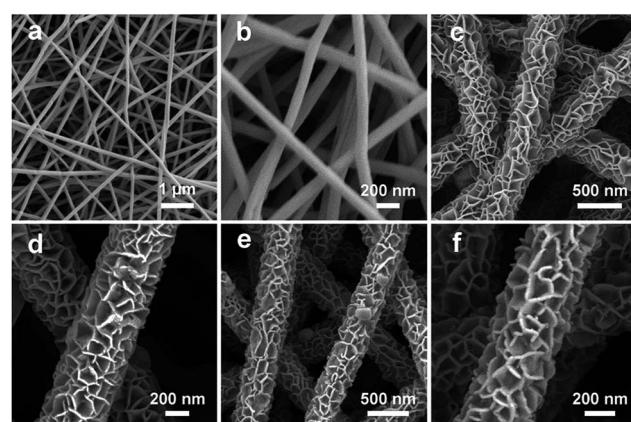

Fig. 2 FESEM images of (a, b) carbon nanofiber films at different magnifications; (c, d) Ni–Co–O precursor nanosheets grown on carbon nanofibers at different magnifications; (e, f) $NiCo_2O_4$ nanosheets grown on carbon nanofibers at different magnifications.

This journal is © The Royal Society of Chemistry 2017

J. Mater. Chem. A, 2017, **5**, 14530–14536 | 14531
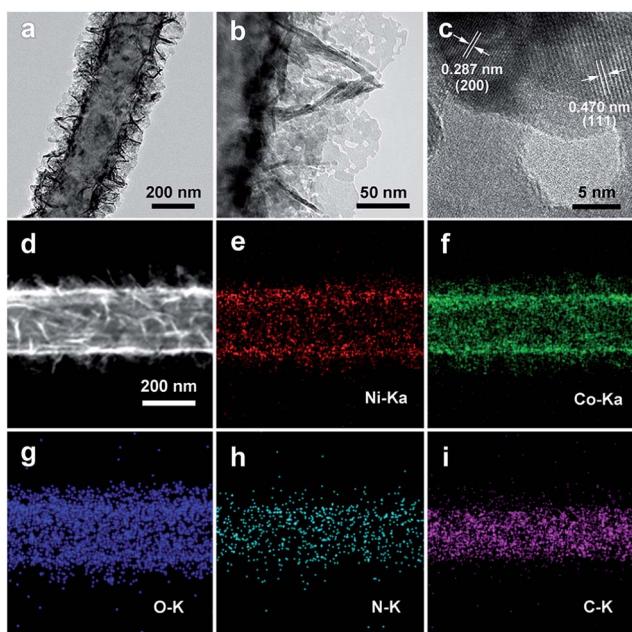
Fig. 3 (a, b) Typical TEM images of NiCo$_2$O$_4$ nanosheets on carbon nanofiber films at different magnifications; (c) an HRTEM image of NiCo$_2$O$_4$ nanosheets; (d–i) HAADF-STEM and corresponding EDX elemental mappings (Ni, Co, O, N, C) of NiCo$_2$O$_4$@CNFs.

compositions of NiCo$_2$O$_4$@CNFs were further analyzed by energy dispersive X-ray (EDX) spectroscopy (Fig. S4, ESI†). The total mass of Ni, Co, and O is 43.8%, which is slightly higher than the TGA result, which might be caused by the oxygen atoms of CNFs. In virtue of 1D nanofibers and the ultrathin sheet-like subunits, these NiCo$_2$O$_4$@CNFs have a relatively large Brunauer–Emmett–Teller (BET) surface area of about 178 m^2 g^{-1} (N$_2$ adsorption desorption isotherm is given in Fig. S5, ESI†).

To further understand the porous nanosheet structure, transmission electron microscopy (TEM) was performed (Fig. 3). In Fig. 3a and b, it can be clearly observed that NiCo$_2$O$_4$ nanosheets are uniformly grown on the CNFs (Fig. 3a), and the surface of NiCo$_2$O$_4$ contains abundant mesopores (Fig. 3b). Furthermore, the high-resolution TEM (HRTEM, Fig. 3c) images of NiCo$_2$O$_4$ nanosheets exhibits lattice fringes with inter-planar spacings of 0.287 nm and 0.470 nm, corresponding to the (200) and (111) planes of NiCo$_2$O$_4$. Energy-dispersive X-ray (EDX) mapping was used to further analyze the distribution of the catalyst on CNFs, as shown in Fig. 3d–i. The Ni, Co, and O elements are uniformly distributed around a carbon nanofiber, and the C element is distributed into the core of the composite. In addition, energy dispersive X-ray (EDX, Fig. S6, ESI†) spectral line-scan results show that the C element is mainly detected
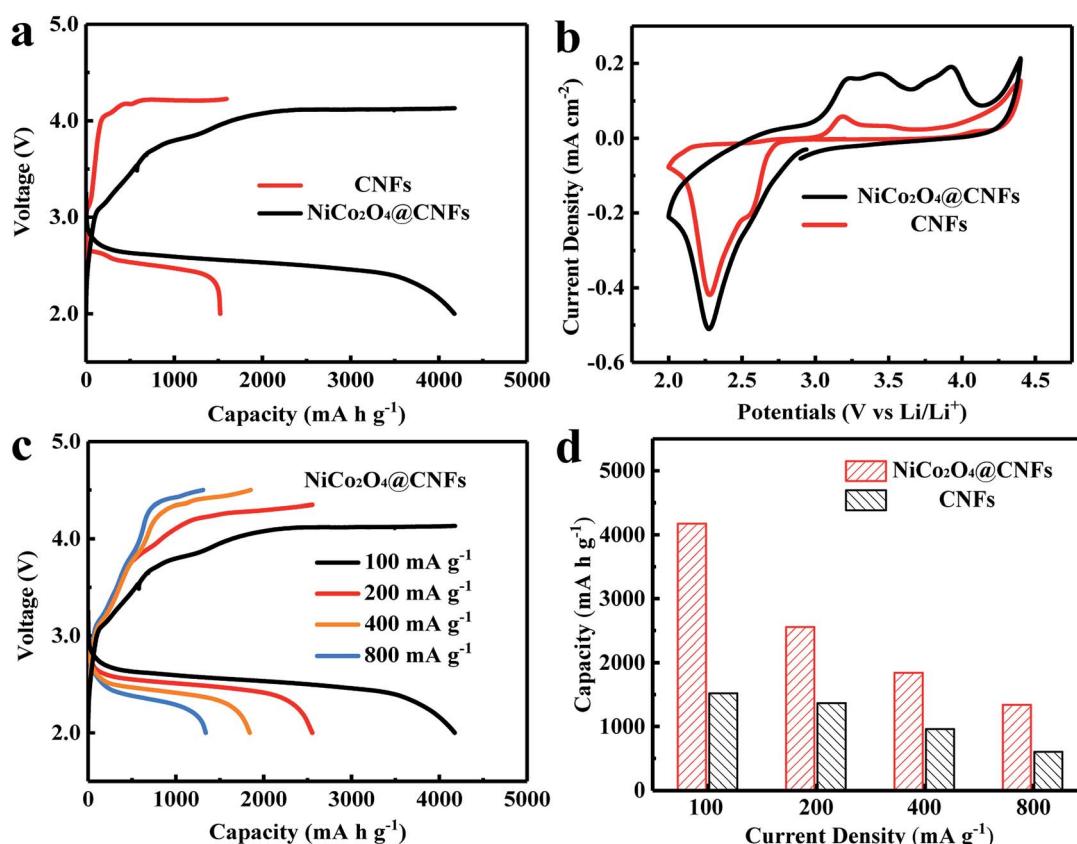
Fig. 4 (a) Initial discharge/charge curves of Li–O$_2$ batteries with NiCo$_2$O$_4$@CNFs and CNFs cathodes at a current density of 100 mA g^{-1}; (b) CV curves of NiCo$_2$O$_4$@CNFs and CNFs cathodes between 2.0 and 4.5 V at 0.1 mV s^{-1}; (c) discharge/charge curves of Li–O$_2$ batteries with the NiCo$_2$O$_4$@CNFs cathode at various current densities; (d) the rate capability of Li–O$_2$ batteries with NiCo$_2$O$_4$@CNFs and CNFs cathodes at various current densities.

inside the NiCo$_2$O$_4$@CNFs, and the Ni, Co, and O elements are mainly detected on the shell, which could suggest that the CNFs are covered by a uniform coating layer of NiCo$_2$O$_4$.[45]

We subsequently investigated the electrochemical properties of the NiCo$_2$O$_4$@CNFs as a cathode for Li–O$_2$ batteries. Fig. 4a shows the discharge–charge voltage profiles of NiCo$_2$O$_4$@CNFs and CNFs cathodes at a current density of 100 mA g^{-1}. The NiCo$_2$O$_4$@CNFs cathode shows a high initial discharge capacity of 4179 mA h g^{-1}, which is higher than that of the CNFs cathode (1591 mA h g^{-1}). Furthermore, the NiCo$_2$O$_4$@CNFs cathode presents lower overpotentials than CNFs, which suggests that the NiCo$_2$O$_4$ catalyst has higher electrocatalytic activities toward the ORR/OER.[46,47] The NiCo$_2$O$_4$@CNFs cathode with different loading masses at the same mass current density was investigated as shown in Fig. S7.† The specific capacities of the NiCo$_2$O$_4$@CNFs cathode with loading masses of 0.134, 0.268, and 0.536 mg cm^{-2} were 4179, 2231, and 1992 mA h g^{-1}, respectively. The morphological changes of the NiCo$_2$O$_4$@CNFs cathode after the 1st full discharge and 1st charge are examined (Fig. S8, ESI†). As shown Fig. S8b, ESI,† the NiCo$_2$O$_4$ shell is constructed by nanosheet-like subunits on the carbon nanofibers. The part of 3D spaces with NiCo$_2$O$_4$ nanosheets was filled with the discharge product (Li$_2$O$_2$) during the discharge process from 0 mA h g^{-1} to 1000 mA h g^{-1} (Fig. S8c, ESI†). Then, the 3D structure was completely covered by the discharge product after being discharged to 2.0 V (Fig. S8d, ESI†). After the charge

process, the 3D structure consisting of porous NiCo$_2$O$_4$ nanosheets was still observed obviously (Fig. S8e, ESI†) suggesting that the NiCo$_2$O$_4$@CNFs can remain stable enough during the discharge and charge processes and the discharge product inside the 3D structure was decomposed completely after charging, which suggest that the NiCo$_2$O$_4$@CNFs cathode show good mass transfer channels during the discharge and charge processes enhancing its capacity and recovery.[47] In order to further investigate the electrocatalytic activities of the NiCo$_2$O$_4$@CNFs, cyclic voltammetry (CV) was performed at a scan rate of 0.1 mV s^{-1} in the voltage window of 2.0–4.5 V, as shown in Fig. 4b. The CV behaviors are similar to those previously reported, suggesting that the oxygen electrodes have the same reaction pathway.[23,46,48] Specifically, one reduction peak can be clearly observed, which can be ascribed to the oxygen reduction. In addition, the NiCo$_2$O$_4$@CNFs cathode exhibits a lower onset ORR potential and larger ORR peak current density than CNFs. Consistent with the result of the discharge–charge profile, the CV curve of the NiCo$_2$O$_4$@CNFs cathode shows three oxidation peaks at around 3.24, 3.44, and 3.93 V, respectively, which is attributed to the stepwise process of decomposition of Li$_2$O$_2$.[14,48,49] Moreover, the NiCo$_2$O$_4$@CNFs cathode shows a higher OER peak current density than CNFs. The rate capability of the NiCo$_2$O$_4$@CNFs and CNFs cathodes was investigated through galvanostatic discharge–charge at various current densities from 100 to 800 mA g^{-1}, as shown in Fig. 4c
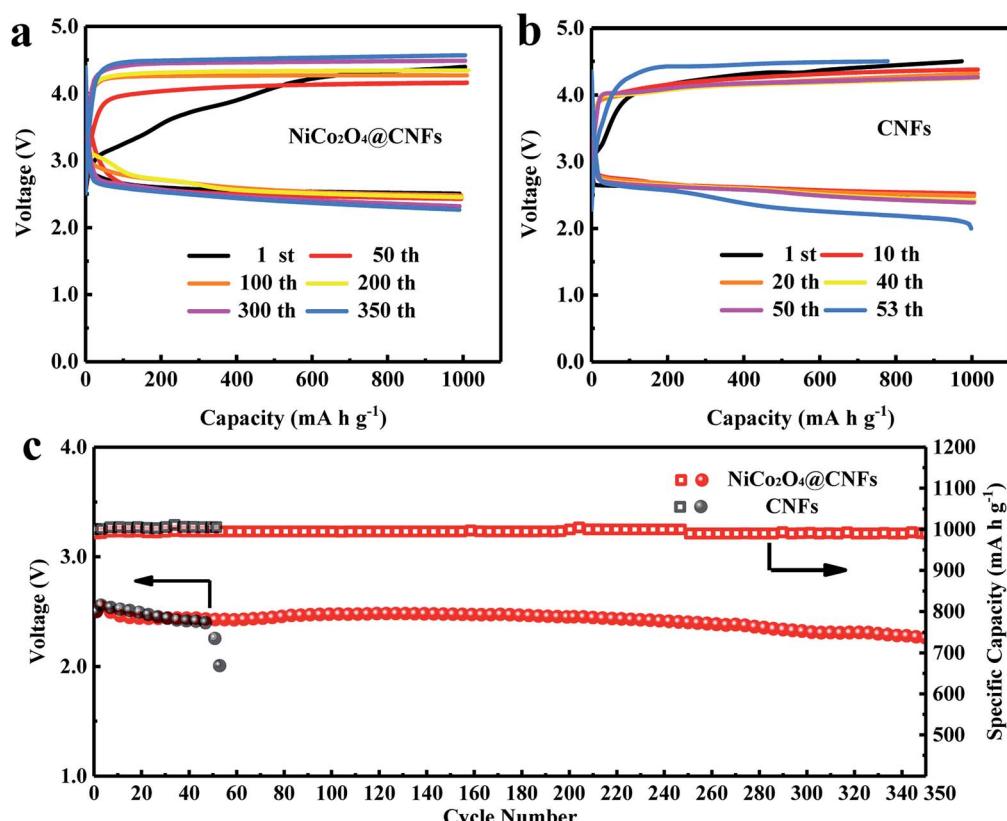

Fig. 5   (a and b) The cycling performance of NiCo$_2$O$_4$@CNFs and CNFs cathodes at a current density of 200 mA g^{-1} and a specific capacity limit of 1000 mA h g^{-1}; (c) the terminal discharge voltage as a function of cycle number for Li–O$_2$ batteries with NiCo$_2$O$_4$@CNFs and CNFs cathodes.

and d. The NiCo$_2$O$_4$@CNFs cathode delivers a high discharge capacity of 1339 mA h g^{-1} with a corresponding coulombic efficiency (CE) of 97.8% at a high current density of 800 mA g^{-1} (Fig. 4c), while the discharge capacity of the CNFs is 603 mA h g^{-1} with a CE of 74.5% at 800 mA g^{-1} (Fig. S9, ESI†).

The cycling tests of Li–O$_2$ batteries were performed to evaluate the long-term catalytic activity of the NiCo$_2$O$_4$@CNFs cathode. The cycling performance was tested at a current density of 200 mA g^{-1} with a fixed specific capacity of 1000 mA h g^{-1} (Fig. 5). As shown in Fig. 5a and b, the NiCo$_2$O$_4$@CNFs cathode shows lower ORR/OER overpotentials and a higher energy efficiency than the CNFs cathode. As shown in Fig. 5c, the terminal discharge voltage of the NiCo$_2$O$_4$@CNFs cathode is still above 2.0 V even after 350 cycles. In contrast, the terminal discharge voltage of the CNFs cathode declines to under 2.0 V after only 53 cycles. In addition, to further investigate the stability of the NiCo$_2$O$_4$@CNFs cathode, the morphologies of the cathode were characterized by SEM after discharge and charge cycles, as shown in Fig. S10.† The NiCo$_2$O$_4$ nanosheets on CNFs still have a good structure after the cycles. The full discharge–charge curves of the Li–O$_2$ battery with the NiCo$_2$O$_4$@CNFs cathode are shown in Fig. S11 (ESI†). The NiCo$_2$O$_4$@CNFs cathode exhibits low overpotentials, especially a charge potential of under 4.0 V in Fig. S11a (ESI†). In addition, the NiCo$_2$O$_4$@CNFs cathode achieves the highest capacity of 7168 mA h g^{-1} in the 18th cycle and still maintains a high capacity of 5738 mA h g^{-1} after 20 full cycles (Fig. S11b, ESI†). The excellent cycling stability indicates that the NiCo$_2$O$_4$@CNFs cathode maintains a good bi-functional catalytic activity for a long time.[8,46,47]

Compared with reported NiCo$_2$O$_4$ based cathodes (Table S1, ESI†), it is worth mentioning that the Li–O$_2$ battery performance of the NiCo$_2$O$_4$@CNFs cathode is significantly outstanding, including its cycling stability and capacity. Meanwhile, the relationship between the discharge capacity and cycle performance of reported cathodes is shown in Fig. 6a. The Li–O$_2$ battery performance of the NiCo$_2$O$_4$@CNFs cathode is much better than those of the reported binder-free cathode. It should be noticed that the NiCo$_2$O$_4$@CNFs cathode shows better cycling performance despite lower initial discharge capacity than the binder-added cathodes. Furthermore, the NiCo$_2$O$_4$@CNFs cathode exhibits an extremely high energy density of 2110 W h kg^{-1}, which is much higher than that of reported Li–O$_2$ batteries (Fig. 6b).[17,23,24,39,50]

The excellent cycling performance and high energy density of the NiCo$_2$O$_4$@CNFs cathode might be attributed to the rational design and engineering of catalysts and porous conductive electrodes.[47] Specifically, compared with the binder-free NiCo$_2$O$_4$-based cathode (<6 wt%) in Table S1,† the hierarchical nanostructures with a high NiCo$_2$O$_4$ loading mass (40 wt%) could provide more active sites for the ORR/OER and spaces for Li$_2$O$_2$ formation and deposition during cycling processes. In addition, the low-dimensional NiCo$_2$O$_4$ nanosheets facilitate Li$^+$/O$_2$ transfer on the shell structure. Meanwhile, the NiCo$_2$O$_4$ shell on CNFs could prevent the side reaction between carbon and intermediates at high potential.[8,19,45] Furthermore, the "binder-free" NiCo$_2$O$_4$@CNFs
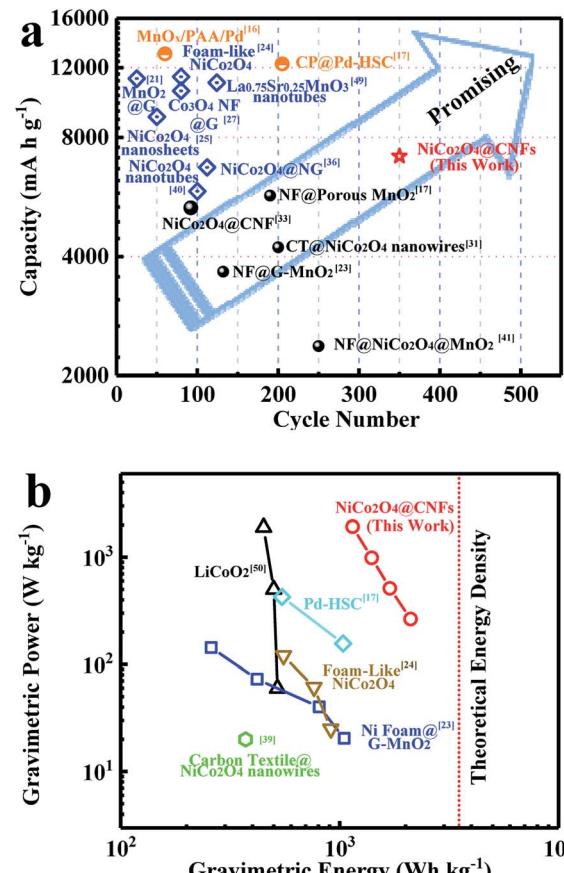
Fig. 6 (a) Initial full discharge capacity and cycle performance limited capacity results of previously reported studies based on oxygen electrodes (blue rhombus: organic binder; black solid circle: binder-free; orange circle: noble metal electrodes); (b) gravimetric energy and power of various oxygen electrodes compared with those of LiCoO$_2$ (NF: Ni foam; CT: carbon textile).

cathode with highly conducive CNFs also avoids binder-induced problems, such as the side reaction of organic binder decomposition.[23,44,48] Thus, combining the hierarchical NiCo$_2$O$_4$ nanostructure and porous conductive electrode, the NiCo$_2$O$_4$@CNFs cathode exhibits high capacity and excellent cycling performance. Simultaneously, with the low mass density of the porous conductive electrode (CNFs) in NiCo$_2$O$_4$@CNFs, an extremely high energy density of 2110 W h kg^{-1} can be achieved.

Conclusions

In summary, hierarchical NiCo$_2$O$_4$ nanosheets grown on carbon nanofiber films were synthesized *via* a hydrothermal method followed by annealing treatment as binder free cathodes for Li–O$_2$ batteries. The NiCo$_2$O$_4$@CNFs cathode simultaneously integrates an efficient bifunctional catalyst with a rationally designed electrode for long life, high energy density Li–O$_2$ batteries based on low-dimensional ultrathin nanosheets, lightweight conductive carbon networks, and a binder-free cathode. When evaluated as a cathode for Li–O$_2$ batteries, the NiCo$_2$O$_4$@CNFs electrode can manifest high specific capacity,

14534 | *J. Mater. Chem. A*, 2017, **5**, 14530–14536

This journal is © The Royal Society of Chemistry 2017

high energy density and excellent cycling stability. From these results, the rational design of the hierarchical catalyst constructed low-dimensional nanostructure and the lightweight porous carbon nanofiber electrode toward oxygen cathodes can be also used for other metal–oxygen batteries, such as Zn–O_2 batteries, Al–O_2 batteries, and Na–O_2 batteries.

Acknowledgements

Notes and references

1 P. G. Bruce, S. A. Freunberger, L. J. Hardwick and J. M. Tarascon, *Nat. Mater.*, 2012, **11**, 19.
2 N. Feng, P. He and H. Zhou, *Adv. Energy Mater.*, 2016, **6**, 201502303.
3 Y. Y. Shao, F. Ding, J. Xiao, J. Zhang, W. Xu, S. Park, J. G. Zhang, Y. Wang and J. Liu, *Adv. Funct. Mater.*, 2013, **23**, 987.
4 Y. Li, X. Wang, S. Dong, X. Chen and G. Cui, *Adv. Energy Mater.*, 2016, **6**, 201600751.
5 G. Girishkumar, B. McCloskey, A. C. Luntz, S. Swanson and W. Wilcke, *J. Phys. Chem. Lett.*, 2010, **1**, 2193.
6 J. Lu, L. Li, J. B. Park, Y. K. Sun, F. Wu and K. Amine, *Chem. Rev.*, 2014, **114**, 5611.
7 W. B. Luo, X. W. Gao, D. Q. Shi, S. L. Chou, J. Z. Wang and H. K. Liu, *Small*, 2016, **12**, 3031.
8 K. Liao, X. Wang, Y. Sun, D. Tang, M. Han, P. He, X. Jiang, T. Zhang and H. Zhou, *Energy Environ. Sci.*, 2015, **8**, 1992.
9 L. Grande, E. Paillard, J. Hassoun, J. B. Park, Y. J. Lee, Y. K. Sun, S. Passerini and B. Scrosati, *Adv. Mater.*, 2015, **27**, 784.
10 J. Wang, Y. Li and X. Sun, *Nano Energy*, 2013, **2**, 443.
11 Z. W. Chang, J. J. Xu, Q. C. Liu, L. Li and X. B. Zhang, *Adv. Energy Mater.*, 2015, **5**, 201500633.
12 A. Kraytsberg and Y. Ein-Eli, *J. Power Sources*, 2011, **196**, 886.
13 J. S. Lee, S. T. Kim, R. Cao, N. S. Choi, M. Liu, K. T. Lee and J. Cho, *Adv. Energy Mater.*, 2011, **1**, 34.
14 Y. C. Lu, B. M. Gallant, D. G. Kwabi, J. R. Harding, R. R. Mitchell, M. S. Whittingham and S. H. Yang, *Energy Environ. Sci.*, 2013, **6**, 750.
15 Z. Peng, S. A. Freunberger, Y. Chen and P. G. Bruce, *Science*, 2012, **337**, 563.
16 D. Oh, J. F. Qi, Y. C. Lu, Y. Zhang, S. H. Yang and A. M. Belcher, *Nat. Commun.*, 2013, **4**, 2756.
17 J. J. Xu, Z. L. Wang, D. Xu, L. L. Zhang and X. B. Zhang, *Nat. Commun.*, 2013, **4**, 2438.
18 Y. C. Lu, Z. C. Xu, H. A. Gasteiger, S. Chen, H. S. Kimberly and S. H. Yang, *J. Am. Chem. Soc.*, 2010, **132**, 12170.
19 F. J. Li, D. M. Tang, Z. L. Jian, D. Q. Liu, D. Golberg, A. Yamada and H. S. Zhou, *Adv. Mater.*, 2014, **26**, 4659.
20 A. Débart, A. J. Paterson, J. Bao and P. G. Bruce, *Angew. Chem., Int. Ed.*, 2008, **120**, 4597.
21 Y. Cao, Z. Wei, J. He, J. Zang, Q. Zhang, M. Zheng and Q. Dong, *Energy Environ. Sci.*, 2012, **5**, 9765.
22 X. Hu, F. Cheng, X. Han, T. Zhang and J. Chen, *Small*, 2015, **11**, 809.
23 S. Liu, Y. Zhu, J. Xie, Y. Huo, H. Y. Yang, T. Zhu, G. Cao, X. Zhao and S. Zhang, *Adv. Energy Mater.*, 2014, **4**, 201301960.
24 L. L. Liu, J. Wang, Y. Y. Hou, J. Chen, H. K. Liu, J. Z. Wang and Y. P. Wu, *Small*, 2016, **12**, 602.
25 B. Sun, X. Huang, S. Chen, Y. Zhao, J. Zhang, P. Munroe and G. Wang, *J. Mater. Chem. A*, 2014, **2**, 12053.
26 Y. Liang, Y. Li, H. Wang, J. Zhou, J. Wang, T. Regier and H. Dai, *Nat. Mater.*, 2011, **10**, 780.
27 W. H. Ryu, T. H. Yoon, S. H. Song, S. Jeon, Y. J. Park and I. D. Kim, *Nano Lett.*, 2013, **13**, 4190.
28 T. Y. Ma, S. Dai, M. Jaroniec and S. Z. Qiao, *J. Am. Chem. Soc.*, 2014, **136**, 13925.
29 D. Oh, J. F. Qi, B. H. Han, G. R. Zhang, T. J. Carney, J. Ohmura, Y. Zhang, S. H. Yang and A. M. Belcher, *Nano Lett.*, 2014, **14**, 4837.
30 H. Wang, Y. Yang, Y. Liang, G. Zheng, Y. Li, Y. Cui and H. Dai, *Energy Environ. Sci.*, 2012, **5**, 7931.
31 S. Peng, L. Li, Y. Hu, M. Srinivasan, F. Cheng, J. Chen and S. Ramakrishna, *ACS Nano*, 2015, **9**, 1945.
32 C. Li, X. P. Han, F. Y. Cheng, Y. X. Hu, C. C. Chen and J. Chen, *Nat. Commun.*, 2015, **6**, 7345.
33 S. X. Liu, L. F. Hu, X. J. Xu, A. A. Al-Ghamdi and X. S. Fang, *Small*, 2015, **11**, 4267.
34 Z. Gao, W. Yang, J. Wang, N. Song and X. Li, *Nano Energy*, 2015, **13**, 306.
35 G. Zhang and X. W. Lou, *Adv. Mater.*, 2013, **25**, 976.
36 H. Gong, H. R. Xue, T. Wang, H. Guo, X. L. Fan, L. Song, W. Xia and J. P. He, *ACS Appl. Mater. Interfaces*, 2016, **8**, 18060.
37 H. Xue, X. Mu, J. Tang, X. Fan, H. Gong, T. Wang, J. He and Y. Yamauchi, *J. Mater. Chem. A*, 2016, **4**, 9106.
38 Y. Luo, F. L. Lu, C. Jin, Y. R. Wang, R. Z. Yang and C. H. Yang, *J. Power Sources*, 2016, **319**, 19.
39 H. R. Xue, S. C. Wu, J. Tang, H. Gong, P. He, J. P. He and H. S. Zhou, *ACS Appl. Mater. Interfaces*, 2016, **8**, 8427.
40 L. Y. Li, L. F. Shen, P. Nie, G. Pang, J. Wang, H. S. Li, S. Y. Dong and X. G. Zhang, *J. Mater. Chem. A*, 2015, **3**, 24309.
41 A. Riaz, K. N. Jung, W. Chang, K. H. Shin and J. W. Lee, *ACS Appl. Mater. Interfaces*, 2014, **6**, 17815.
42 J. Xie, X. Yao, Q. Cheng, I. P. Madden, P. Dornath, C. C. Chang, W. Fan and D. Wang, *Angew. Chem., Int. Ed.*, 2015, **54**, 4299.
43 D. Xiao, S. Dong, J. Guan, L. Gu, S. Li, N. Zhao, C. Shang, Z. Yang, H. Zheng, C. Chen, R. Xiao, Y. S. Hu, H. Li, G. Cui and L. Chen, *Adv. Energy Mater.*, 2015, **5**, 1400664.
44 Q. C. Liu, J. J. Xu, D. Xu and X. B. Zhang, *Nat. Commun.*, 2015, **6**, 7892.
45 Z. L. Jian, P. Liu, F. J. Li, P. He, X. W. Guo, M. W. Chen and H. S. Zhou, *Angew. Chem., Int. Ed.*, 2014, **53**, 442.

This journal is © The Royal Society of Chemistry 2017

J. Mater. Chem. A, 2017, **5**, 14530–14536 | **14535**

46 G. Liu, H. Chen, L. Xia, S. Wang, L. X. Ding, D. Li, K. Xiao, S. Dai and H. Wang, *ACS Appl. Mater. Interfaces*, 2015, **7**, 22478.

47 J. J. Xu, D. Xu, Z. L. Wang, H. G. Wang, L. L. Zhang and X. B. Zhang, *Angew. Chem., Int. Ed.*, 2013, **52**, 3887.

48 F. F. Tu, J. Xie, S. C. Zhang, G. S. Cao, T. J. Zhu and X. B. Zhao, *J. Mater. Chem. A*, 2015, **3**, 5714.

49 D. Zhai, H. H. Wang, J. Yang, K. C. Lau, K. Li, K. Amine and L. A. Curtiss, *J. Am. Chem. Soc.*, 2013, **135**, 15364.

50 R. R. Mitchell, B. M. Gallant, C. V. Thompson and S. H. Yang, *Energy Environ. Sci.*, 2011, **4**, 2952.